Excimer Energies

Ruoqi Zhao,[1,2,‡] Christian Hettich,[3,‡] Jun Zhang,[2,*] Meiyi Liu,[2,*] Jiali Gao[2,3*]

[1]*Institute of Theoretical and Computational Chemistry, Jilin University, Changchun, Jilin 130023, China*

[2]*Institute of Systems and Physical Biology, Shenzhen Bay Laboratory, Shenzhen, Guangdong 518055, China*

[3]*Department of Chemistry and Supercomputing Institute, University of Minnesota, Minneapolis, Minnesota 55455, USA*

‡ These authors contributed equally.

* Corresponding authors: e-mails: zhangjun@szbl.ac.cn (JZ), liumy@szbl.ac.cn (ML), gao@jialigao.org (JG),

Abstract: A multistate energy decomposition analysis (MS-EDA) method is introduced for excimers using density functional theory. Although EDA has been widely applied to intermolecular interactions in the ground-state, few methods are currently available for excited state complexes. Here, the total energy of an excimer state is separated into exciton excitation

energy $\Delta E_{Ex}(|\Psi_X \bullet \Psi_Y >^*)$, resulting from the state interaction between locally excited monomer states $|\Psi_X^* \bullet \Psi_Y >$ and $|\Psi_X \bullet \Psi_Y^* >$, a super-exchange resonance energy ΔE_{SE}, originating from the mutual charge transfer between two monomers $|\Psi_X^+ \bullet \Psi_Y^- >$ and $|\Psi_X^- \bullet \Psi_Y^+ >$, and an orbital-and-configuration delocalization term ΔE_{OCD} due to the expansion of configuration space and block-localized orbitals to the fully delocalized dimer system. Although there is no net charge transfer in symmetric excimer cases, the resonance of charge-transfer states is critical to stabilizing the excimer. The monomer localized excited and charge-transfer states are variationally optimized, forming a minimal active space for nonorthogonal state interaction (NOSI) calculations in multistate density functional theory to yield the intermediate states for energy analysis. The present MS-EDA method focuses on properties unique to excited states, providing insights into exciton coupling, super-exchange and delocalization energies. MS-EDA is illustrated on the acetone and pentacene excimer systems; three configurations of the latter case are examined, including the optimized excimer, a stacked configuration of two pentacene molecules and the fishbone orientation. It is found that excited-state energy splitting is strongly dependent on the relative energies of the monomer excited states and the phase-matching of the monomer wave functions.

TOC graphic

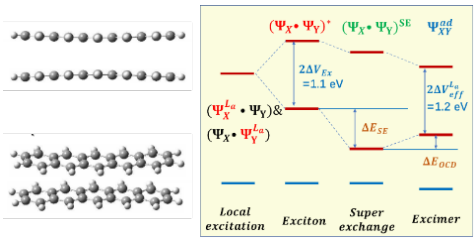
$(\Psi_X \bullet \Psi_Y)^*$
$(\Psi_X \bullet \Psi_Y)^{SE}$
Ψ_{XY}^{ad}
$2\Delta V_{Ex}$ =1.1 eV
$(\Psi_X^{La} \bullet \Psi_Y)$&
$(\Psi_X \bullet \Psi_Y^{La})$
ΔE_{SE}
$2\Delta V_{eff}^{La}$ =1.2 eV
ΔE_{OCD}
Local excitation
Exciton
Super exchange
Excimer

Energy decomposition analysis (EDA) is a useful tool for understanding intermolecular interactions.[1-3] Although methods for molecular complexes in the ground state have been thoroughly developed,[4-55] few approaches are currently available for analyzing energy terms of excimers and exciplexes – molecular aggregates formed in the electronic excited states. One exception is a study by Ge et al.,[56, 57] who used the same energy terms in ground-state EDA,[2, 49] including frozen (frz), polarization (pol) and charge transfer (CT) terms to describe intermolecular interactions in the excited states $\Delta E^*_{\mathrm{int}} = \Delta E^*_{\mathrm{frz}} + \Delta E^*_{\mathrm{pol}} + \Delta E^*_{\mathrm{CT}}$. The method was introduced on the basis of configuration interaction with singly excitations (CIS), in principle, extendable to time-dependent density functional theory (TDDFT) for excited-state calculations. In particular, the frozen excitation energy was obtained with the use of fixed orbitals of each isolated fragment along with its excitation amplitudes, and frozen interactions were modeled through the merged Fock matrix. Similarly, polarization contribution was determined with the relaxed, fragment block-localized molecular orbitals (BLMO) also called absolutely localized MOs.[24, 25, 27, 28, 58] The CT term was simply the difference between the excitation energy of the full complex and the other two terms. That work was extended to excimers with the addition of an exciton splitting term between the frozen excited states.[59] That work provided an analysis of excited state interactions from a ground-state analogy. On the other hand, it is of interest to define variationally optimizable diabatic states,[60-62] such as the local excitations of individual chromophores in the presence of other molecules in the ground stat. Electronic coupling interaction among local states can be used to determine the rates of excited-state energy transfer such as light-harvesting in photosynthesis and perception,[63-66] photoexcitation-induced oxidation-reduction reactions and processes in photovoltaic devices and fuel cells.[67] In this *Letter*, we introduce an alternative, multistate energy-decomposition analysis (MS-EDA) for the interaction energy of an excimer complex – excited-

state complex formed between the same chemical species. We focus on energy terms unique to excited states, including local excitation, exciton excitation ΔE_{Ex}, resonance stabilization due to super-exchange ΔE_{SE}, and orbital and configuration-state delocalization ΔE_{OCD}. The method is illustrated on the acetone and pentacene excimers, relevant to chemiluminescence and singlet fission in materials for solar cells.[67, 68]

Considering the following photochemical process of excimer formation,

$$X + Y \xrightarrow{h\nu} X + Y^* \xrightarrow{\Delta E_b^K} (XY)^* \quad (1)$$

we define the total formation energy, or binding energy, of the excimer $(XY)^*$ in its *K*th excited state relative to that of two separate molecules in the ground state (eq 1) as follows:

$$\Delta E_b^K = E_{(XY)^*}^K\left[\Psi_{(XY)^*}^K\right] - E_X^o[\Psi_X^o] - E_Y^o[\Psi_Y^o] - h\nu \quad (2)$$

where the superscript "*o*" denotes the energy and wave function of a molecule in the ground state, $E_{(XY)^*}^K$ is the energy of the *K*th excited state of the excimer$(XY)^*$, characterized by the wave function$\Psi_{(XY^*)}^K$, and $h\nu$ is the external photoenergy of chromophore excitation. Although the main goal of this study is concerned with excimers, we nevertheless use different symbols *X* and *Y* to denote the two interacting molecules for convenience of discussion. Thus, the theory is generally applicable to exciplexes in which $X \neq Y$. Also, the method can easily be generalized to any number of molecules, suitable for the treatment of delocalized, exciton-resonance excitation of extended materials and biological light-harvesting systems.

Multistate energy-decomposition analysis (MS-EDA). We partition the total binding interaction energy of an excimer complex (eq 2) in its *K*th excited state into the following terms:

$$\Delta E_b^K = \Delta E_{\mathrm{Lint}}[(X \bullet Y)] - h\nu + \Delta E_{\mathrm{Ex}}^K[(X \bullet Y)^*] + \Delta E_{\mathrm{SE}}^K\left[\left(X^{\pm} \bullet Y^{\mp}\right)^*\right] + \Delta E_{\mathrm{OCD}}^K[(XY)^*] \quad (3)$$

where $\Delta E_{\mathrm{Lint}}[(X \bullet Y)]$ denotes the local interaction energy between monomers *X* and *Y* in the ground state, $\Delta E_{\mathrm{Ex}}^K[(X \bullet Y)^*]$ is the excitation energy of the *K*th exciton state (Ex) due to

resonance delocalization of local, monomer excitations, $\Delta E_{\mathrm{SE}}^{K}\left[\left(X^{\pm} \bullet Y^{\mp}\right)^{*}\right]$ specifies the effect of inter-fragment charge-transfer configurations called super-exchange (SE), and $\Delta E_{\mathrm{OCD}}^{K}[(XY)^{*}]$ represents the energy change due to orbital and configuration-state delocalization (OCD) by expansion from monomer BLMOs to the full molecular space. The progressive sequence of intermediate states depicted in Scheme 1 have well-defined wave functions (or Kohn-Sham states) which can be variationally optimized, and the decomposed energy terms sum up exactly to the definition of eq 2.

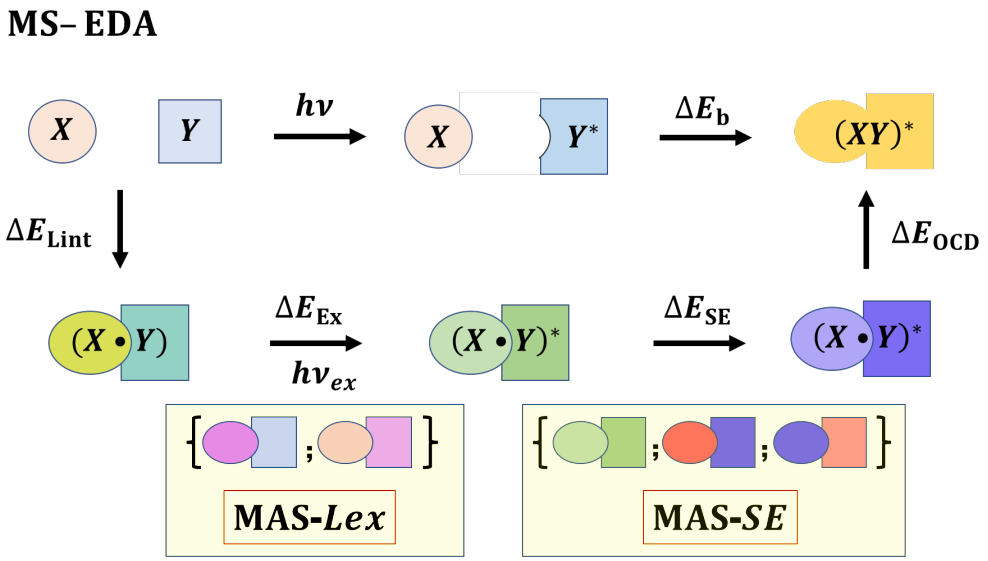

Scheme 1. Multistate energy decomposition analysis (MS-EDA) of the excimer binding energy ΔE_b. The top row corresponds to the physical process of excimer formation (eq 2). The remaining illustration highlights each energy terms defined by eq 3 and their progressive change in MS-EDA. The shapes of objects represent molecular geometries, while different colors depict the corresponding wave functions with boundaries shown for block-localization. All wave functions can be variationally optimized. The local excited in pink (Lex) and charge transfer diabatic states in light yellow background denote the minimum active space (MAS) for the exciton and super-exchange states. The energy changes are defined by eq 4 for the local interaction energy ΔE_{Lint}, eq 6 for the exciton excitation energy ΔE_{Ex}, eq 9 for the super-exchange stabilization energy ΔE_{SE}, and eq 10 for the orbital and configuration delocalization effects ΔE_{OCD}. The definition of the respective wave functions can also be found in these equations.

Local interaction energy in the ground state. For analysis of excited-state energies in MS-EDA, we focus on the energy terms that are directly related to the excimer complex. Therefore, all

energy contributions that can be associated with intermolecular interactions between monomers *X* and *Y* in the ground state are grouped into a single term called local interaction (Lint) energy.

$$\Delta E_{\mathrm{Lint}}[(X \bullet Y)] = E_{(X \bullet Y)}\left[\Psi_{(X \bullet Y)}\right] - E_X^o[\Psi_X^o] - E_Y^o[\Psi_Y^o] \quad (4)$$

where the notation $(X \bullet Y)$ separating monomers *X* and *Y* by the symbol "$\bullet$" represents a block-localized bimolecular complex, and the parentheses indicate that the product wave function of the monomers (ground or excited states) is antisymmetrized, e.g., $\Psi_{(X \bullet Y)} = \hat{A}\{\Psi_X \Psi_Y\}$. This convention is used throughout this *Letter*. We note that the molecular geometry used to determine $E_{(X \bullet Y)}\left[\Psi_{(X \bullet Y)}\right]$ is that of the excimer complex, not the structure optimized for the ground state.

The term "block-local" refers to the strict localization of molecular orbitals (BLMO)[28] in WFT or Kohn-Sham orbitals in DFT (BLKS) in the complex $(X \bullet Y)$.[69] They are strictly localized within the two individual molecular fragments because BLMOs are expanded over basis orbitals on the atoms in each monomer.[28] $\Delta E_{\mathrm{Lint}}[(X \bullet Y)]$ includes classical Coulomb interaction, quantum-mechanical exchange-repulsion and polarization energies, plus the energy change from the equilibrium geometries of isolated monomers to that in the excimer. This classification follows exactly the convention used in the BLW-ED analysis, similar to other ground-state EDA models.[2, 28, 49] It is identical to the total binding energy of the complex (*XY*), at the given geometry, without the charge-transfer term.[2] Since these are ground-state properties which have been thoroughly explored in the past,[2, 3, 18, 24] we do not further separate and discuss them in this work. Specific details may be found in references [2, 28, 49].

Exciton excitation energy. According to Frenkel exciton model,[70] the resonance excitation (exciton) of an extended system (excimer in this work) results from the interaction of locally (monomer) excited states. The wave function for this intermediate state, or simply an exciton state,

denoted as $(X \bullet Y)^*$, is determined by nonorthogonal state interaction (NOSI)[71, 72] in multistate density functional theory (MSDFT):[73, 74]

$$\Psi^K_{(X\bullet Y)^*} = a_1 \Psi^{K_X}_{(X^*\bullet Y)} + a_2 \Psi^{K_Y}_{(X\bullet Y^*)} \quad (5)$$

where the superscript specifies the *K*th excited state of the exciton, $\Psi^{K_X}_{(X^*\bullet Y)}$ and $\Psi^{K_Y}_{(X\bullet Y^*)}$ represent, respectively, the wave functions of the two locally excited monomers in the presence of the other species in the ground state ($\Psi^{K_X}_{(X^*\bullet Y)} = |\Phi^*_X \Theta_Y >$ and $\Psi^{K_Y}_{(X\bullet Y^*)} = |\Phi_X \Theta^*_Y >$), and a_1 and a_2 are the state coefficients. The states K_X and K_Y of $\Psi^{K_X}_{(X^*\bullet Y)}$ and $\Psi^{K_Y}_{(X\bullet Y^*)}$ correspond to those that contribute to the exciton state *K*. Note that $\Psi^{K_X}_{(X^*\bullet Y)}$ and $\Psi^{K_Y}_{(X\bullet Y^*)}$ themselves, in fact, are generally multiconfigurational wave functions, and more than one state from each monomer may contribute.

The energy difference between the exciton state and the block-localized molecular complex, i.e., the exciton-excitation energy ΔE^K_{Ex}, corresponds to the transition from the ground state of the monomer complex $(X \bullet Y)$ to the exciton resonance state $(X \bullet Y)^*$:

$$\Delta E^K_{\mathrm{Ex}} = E^K_{(X\bullet Y)^*} - E_{(X\bullet Y)} \quad (6)$$

where $E^K_{(X\bullet Y)^*}$ and $E_{(X\bullet Y)}$ are, respectively, the energies of the exciton state $\Psi^{\mathrm{K}}_{\mathrm{Ex}} \equiv \Psi^K_{(X\bullet Y)^*}$ and the ground state $\Psi_{(X\bullet Y)}$

The wave function for the exciton state (eq 5) can be variationally optimized by using a multiconfiguration self-consistent-field (MC-SCF) approach or configuration interaction such as CIS and nonorthogonal configuration interaction (NOCI), also called mixed molecular orbital and valence bond (MOVB) in WFT.[75, 76] Alternatively, they can be obtained from multistate SCF (MS-SCF)[77] and NOSI methods in MSDFT. NOSI is used in the present study, in which we first determine the locally excited states for monomer *X** in the presence of *Y* in its ground state, and monomer *Y** in *X*, respectively, using the block-localized excitation (BLE) method to variationally optimize $\Psi^{K_X}_{(X^*\bullet Y)}$ and $\Psi^{K_Y}_{(X\bullet Y^*)}$ along with the M06-2X functional.[78-80] Then, we construct the

Hamiltonian matrix functional, and the state coefficients a_1 and a_2 in eq 5 are obtained by diagonalizing the NOSI Hamiltonian matrix.[69]

Importantly, the structure weight for each of the locally excited states in the resonance exciton state can be evaluated according to the Chirgwin-Coulson scheme:[81]

$$W_{X^*}^K = a_1^2 + a_1 a_2 S_{12} \tag{7a}$$

$$W_{Y^*}^K = a_1^2 + a_1 a_2 S_{12} \tag{7b}$$

where S_{12} is the overlap integral between the two locally excited states, $S_{12} = S_{21} = \int dr \left\{\Psi_{(X^*\bullet Y)}^{K_X}\right\}^* \Psi_{(X\bullet Y^*)}^{K_Y}$.

Charge transfer states and super-exchange energy. The exciton states above from state interactions among locally excited monomers do not explicitly account for charge-transfer (CT) delocalization in the full system. Often, the energies of CT states between monomers *X* and *Y* are relatively high relative to valent excitations, but they, nevertheless, play an important role in stabilizing the excited complex. If the two monomers are symmetrically equivalent in an excimer, there is no net charge transfer, but the stabilization energy due to the resonance between CT configurations can still be significant. Such a resonance effect is also called super-exchange (SE) interaction in electron transfer theory,[82] which is adopted here. The charge-resonance SE states are given by $\Psi_{\mathrm{SE}} = b_2' |X^+ \bullet Y^- > \pm b_3' |X^- \bullet Y^+ >$, or simply denoted by $\Psi_{\mathrm{SE}} = b_2' \Psi_{\mathrm{FCT}} \pm b_3' \Psi_{\mathrm{BCT}}$ between the $X \rightarrow Y$ forward (FCT) and $Y \rightarrow X$ backward (BCT) CT states.

Here, we define the SE-stabilized intermediate state by the wave function

$$\Psi_{\mathrm{SE}}^K = b_1 \Psi_{(X\bullet Y)^*}^K + b_2 \Psi_{\mathrm{FCT}} \pm \mathrm{b}_3 \Psi_{\mathrm{BCT}} \tag{8}$$

where different coefficients for the two CT states have been used in case $X \neq Y$, in which a single, directional CT state may dominate in an exciplex complex. In this regard, it is of interest to distinguish the term charge transfer, representing a specific, directional CT diabatic state, from

super-exchange which describes a physical property, a resonance-stabilization interaction of the intermediate state. In eq 8, we have assumed that the order of excited states has not changed due to mixing with the CT states. This assumption is purposely for the convenience of expression; in practice, the correct state must be matched at different decomposition steps.

The net stabilization energy due to the admixture between the exciton and SE states is called the super-exchange energy ΔE^K_{SE}:

$$\Delta E^K_{\mathrm{SE}} = E^K_{\mathrm{SE}}[\Psi^K_{\mathrm{SE}}] - E^K_{\mathrm{Ex}}[\Psi^K_{(X\bullet Y)^*}] \tag{9}$$

Analogous to the exciton intermediate state, Ψ^K_{Ex} can be obtained from NOCI in WFT and NOSI in MSDFT.[73, 77] In principle, TDDFT and an MCSCF method could be used in both exciton and super-exchange steps, but it can be rather complicated with nonorthogonal orbitals between different fragment blocks. This is easily accomplished in MSDFT employing NOSI.[78, 79]

Orbital delocalization. So far, the wave functions (or Kohn-Sham determinants) for the intermediate states have been constructed on the basis of fragmental BLMOs. Although incorporation of the SE effects introduces charge delocalization, the charge density is generally not sufficiently relaxed. Furthermore, the intermediate states decomposed at this point may have not included all configurational state functions used to determine the energies of the adiabatic excimer complex $(XY)^*$. Therefore, in the final step of the MS-EDA method, we release the monomeric block-localization constraints and use the fully delocalized molecular orbitals to obtain the energies of the excited states for the excimer complex. These states are denoted as $\Psi^K_{(XY)^*}$ without the dot "•" separating monomers *X* and *Y*. The energy change in this step is called orbital and configuration-state delocalization (OCD) energy, analogous to, but different from the CT energy term in ground-state EDA models since additional configurational state functions may also be included in the final step.

$$\Delta E^{K}_{\mathrm{OCD}} = E^{K}_{(XY)^*}\left[\Psi^{K}_{(XY)^*}\right] - E^{K}_{\mathrm{SE}}[\Psi^{K}_{\mathrm{SE}}] \tag{10}$$

The present MS-EDA method includes three computational steps: (1) the calculation of excitation energies of monomers, (2) the determination of the reference states for energy analysis for block-localized intermediate states, and (3) the evaluation of excitation energies of the fully delocalized dimer complex. The results from both steps (1) and (3) can be validated by comparison with results from TDDFT or MCSCF calculations as well as experimental data. TDDFT is adopted in this work to determine the excitation energies of the excimers. Thus, MS-EDA may be regarded as an analytical tool to interpret the numerical results from TDDFT calculations.

The adiabatic ground and excited states as well as all intermediate states for energy analysis are obtained from NOSI in multistate density functional theory. NOSI differs from nonorthogonal CI (NOCI) in that dynamic correlation is included in the basis states in the first place. Lu and Gao proved that the Hamiltonian in the subspace spanned by the lowest N eigenstates is a matrix functional $\boldsymbol{\mathcal{H}}[\boldsymbol{D}(\boldsymbol{r})]$ of the multistate density $\boldsymbol{D}(\boldsymbol{r})$,[73] extending Hohenberg-Kohn theorems for the ground state to any number of N states in MSDFT. Significantly, it was proven that $\boldsymbol{D}(\boldsymbol{r})$ can be represented by no more than N^2 determinants, defining an upper bound for the number of determinants in an active space,[73] i.e., a minimal active space (MAS),[71, 72, 77] in excited-state DFT calculations. $\boldsymbol{D}(\boldsymbol{r})$ can be variationally optimized by minimizing the trace of $\boldsymbol{\mathcal{H}}[\boldsymbol{D}(\boldsymbol{r})]$. Then, Diagonalization of $\boldsymbol{\mathcal{H}}$ yields the exact energies for all N adiabatic ground and excited states, provided that the exact correlation matrix functional is known (the Lu-Gao theorems established its existence).[73] As in Kohn-Sham DFT, approximate correlation matrix functionals must be used in MSDFT calculations. The accuracy of the present MSDFT-NOSI method can be validated by comparison with results from TDDFT on systems that it is adequate as in the present case, employing the same correlation density functional.[71, 72]

We focus on the lowest excited states of a monomer species and their interactions in the excimer complex. For the monomers and block-localized excitations in dimers in this work, we found that it is sufficient to just include 5 spin-adapted configurations in the MAS, consisting of the reference (ground) state from KS-DFT and four singly excited configurations from the two highest occupied KS orbitals (HOMO) to the two lowest unoccupied KS orbitals (LUMO). Each of the singly excited KS-determinants is optimized using the BLE technique, a form of ΔSCF method capable of block-localized constraints on the orbitals in the dimer case.[78, 79]

Before presenting the MS-EDA results, we outline the procedure for determining the elements of the Hamiltonian matrix functional $\boldsymbol{\mathcal{H}}[\boldsymbol{D}(\boldsymbol{r})]$. In particular, the diagonal elements $\mathcal{H}_{AA}[\boldsymbol{D}(\boldsymbol{r})]$ are given by the KS-DFT energies of the corresponding determinants for the block-localized, excited configurations as well as that of the Kohn-Sham ground state.

$$\mathcal{H}_{AA} = E_A^{KS}(\Xi_A) \tag{11}$$

where Ξ_A is a determinant constrained to a given orbital occupation, including both the ground state and excited configuration. Specifically, the constrained BLKS-determinant wave function for the block-localized dimeric configuration $(X \bullet Y)$ is written as follows:

$$\Xi_{(X\bullet Y)}^{KS} = \hat{A}\{(\chi_1^X \cdots \chi_{N_X}^X) \bullet (\chi_1^Y \cdots \chi_{N_Y}^Y)\} \tag{12}$$

where $\hat{A}$ is the antisymmetrizer, and χ_j^U is the *j*th block-localized spinorbital of fragment U $(U = X, Y)$, and N_U is the number of electrons. For the four singly excited states in the MAS, one of the two highest occupied orbitals is replaced by one of the two lowest unoccupied orbitals, and Ξ_A is optimized individually using the BLE method for the non-aufbau configurations.[78] Note that "state" in this *Letter* refers to a spin-adapted wave function representing the exact density by incorporating dynamic correlation with BLKS-DFT; it is different from a determinant configuration.

The transition density functional (TDF),[83] i.e., the correlation energies for the off-diagonal matrix elements of $\boldsymbol{\mathcal{H}}[\boldsymbol{D}(\boldsymbol{r})]$, can be determined rigorously among spin-complement configurations to yield the spin-adapted states. For example, the TDF correlation energy for the spin-adapted singlet state is obtained in an NOSI calculation with the constraint that the energy of the triplet state $|1,0>$ is identical to that of the $|1,1>$ state.[71, 84, 85] Notice that the latter can be adequately represented by a single determinant, exact in KS-DFT if the KS exchange-correlation functional is exact. Thus, given an approximate density functional approximation used for $\mathcal{H}_{AA}\left[\Xi_A^{\uparrow\downarrow}\right]$ and $\mathcal{H}_{BB}\left[\Xi_B^{\downarrow\uparrow}\right]$ where the arrows indicate the spin of the coupled electrons, the electronic coupling $\mathcal{H}_{AB}[\rho_{AB}]$ to yield the singlet spin-adapted state is uniquely determined by

$$\mathcal{H}_{AB}[\rho_{AB}] = <\Xi_A^{\uparrow\downarrow}\left|\widehat{H}\right|\Xi_B^{\downarrow\uparrow}> + \frac{1}{2}\{E_c^{KS}\left[\rho_T\left(\Xi_T^{\uparrow\uparrow}\right)\right] - E_c^{KS}\left[\rho_A\left(\Xi_A^{\uparrow\downarrow}\right)\right]\} \quad (13)$$

where $E_c^{KS}\left[\rho_T\left(\Xi_T^{\uparrow\uparrow}\right)\right]$ and $E_c^{KS}\left[\rho_A\left(\Xi_A^{\uparrow\downarrow}\right)\right]$ are the correlation energies from KS-DFT using the spin-up triplet determinant $\Xi_T^{\uparrow\uparrow}$, and the spin-mixed determinant $\Xi_A^{\uparrow\downarrow}$ (equivalent with $\Xi_B^{\downarrow\uparrow}$ here).

For the remaining off-diagonal matrix elements, an approximate TDF is needed to account for the dynamic correlation in the electronic coupling between two interacting states. Unlike KS-DFT, an approximate TDF is currently not yet available. In this study, we use an overlap-weighted average correlation energy from KS-DFT for the two individual states Ξ_A and Ξ_B to approximate the TDF correlation term:[69]

$$\mathcal{H}_{AB}[\boldsymbol{D}(\boldsymbol{r})] = <\Xi_A^{KS}\left|\widehat{H}\right|\Xi_B^{KS}> + \frac{1}{2}S_{AB}^{KS}\{E_c^A[\rho_A(\Xi_A^{KS})] + E_c^B[\rho_B(\Xi_B^{KS})]\} \quad (14)$$

where $<\Xi_A^{KS}\left|\widehat{H}\right|\Xi_B^{KS}>$ is obtained using the two BLKS determinant wave functions,[75, 76, 86] Ξ_A^{KS} and Ξ_B^{KS}, for configurations *A* and *B*, S_{AB}^{KS} is their overlap integral, and $E_c^A[\rho_A]$ and $E_c^B[\rho_B]$ are the corresponding correlation energies from the KS approximate density functional. The approximation of eq 14 is the main source of error in MS-EDA.

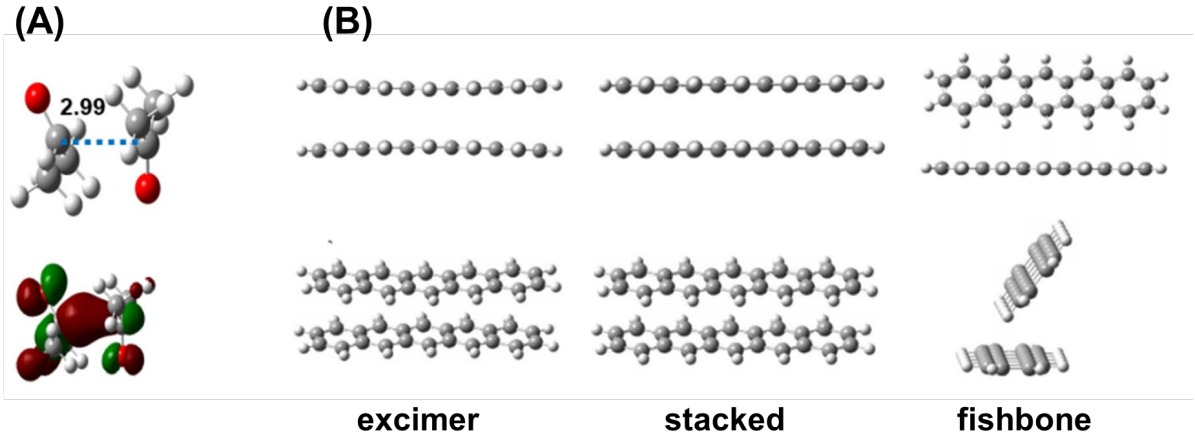

Figure 1. Structures and orbital of excimer complexes. (A). Shown are the optimized structure and the highest singly occupied orbital for the acetone S_1 excimer. (B). Three configurations of pentacene dimer are used in the study, corresponding to the optimized S_1 excimer structure, the on-top stacked configuration of two ground-state pentacene molecules, and a fishbone relative orientation from a pentacene crystal structure.

The MS-EDA method has been implemented in the Qbics program in our laboratories,[87] and a separate BLW-ED program[2] interfaced with the GAMESS-US package.[88] The method and energy terms are illustrated by two excimer complexes: the asymmetric excimer complex of two acetone molecules (Figure 1A), and the pentacene dimer in three different geometry arrangements, including the optimized S_1 excimer, the stacked configuration of two pentacene monomers separated by 3.3 Å, each in the ground state geometry, and the fishbone configuration in the crystal used in an application to singlet fission (Figure 1B).[67] MSDFT-NOSI and TDDFT calculations were carried out using the Minnesota M06-2X density functional[80] along with the cc-pVDZ basis set for the pentacene excimer and cc-pVTZ for the acetone dimer.[89] Geometries were optimized using Gaussian16.[90] Throughout this *Letter*, we use electron volts (eV) as the energy unit to relate with electronic spectroscopy.

Table 1 lists the energies of the ground state and the $n \rightarrow \pi$ excited state from MSDFT-NOSI and TDDFT calculations relative to that from KS-DFT for acetone. The results for the

$L_a(S_1)$ and $L_b(S_2)$ states of pentacene are given in Table 2. The performance of NOSI and possible double counting of electron correlation in a multistate DFT can be validated by comparison of the ground state energies with that from KS-DFT calculations.[83] We find that the difference in ground-state energy between MSDFT and KS-DFT is generally small, with the largest deviation being just -0.02 eV for acetone. Note that the KS-DFT state is included in the active space in all NOSI calculations. This observation indicates that there is little double-counting of correlation in NOSI for the present systems using the M06-2X functional. Importantly, the inclusion of the Kohn-Sham ground-state ensures orthogonality of the computed excited states to the ground state. Listed in Tables 1 and 2 are relative energies for the ground and excited states from NOSI and TDDFT calculations employing monomer geometries optimized for S_0 and S_1 states and monomers in the optimized monomer structure. In addition, we included the computed excitation energies of the excimer complexes. The agreement between NOSI and the linear-response theory is good with a root-mean-square deviation (RMSD) of 0.22 eV, which is largely due to the somewhat greater differences between NOSI and TDDFT for the L_b state of pentacene using M06-2X. If only L_a states of pentacene are included the RMSD error is less than 0.01 eV. Experimental absorption and fluorescence energies for acetone are 4.5 and 2.8 eV in the gas phase,[91] and a acetone excimer fluorescence energy of 3.06 eV has been reported;[92] these results are in good accord with NOSI and TDDFT results in Table 1. The results in Table 1 demonstrate that the MAS used in NOSI for these chromophores is sufficient to represent these states, demonstrating that MS-EDA can be applied to analyze interaction energies of excited-state complexes.

Table 1. Computed energies (eV) for the ground state and the $n \rightarrow \pi^*$ excited state of an acetone molecule. Geometries used include the monomer structure in the ground state (S_0) and the first excited state (S_1), along with the monomers in the optimized dimeric excimer (DM), resembling

the ground and excited state. Energies are determined using nonorthogonal state interaction (NOSI) and time-dependent density functional theory (TDDFT). The Minnesota M06-2X density functional along with the cc-pVTZ basis set is used.

Geometry[a]	NOSI		TDDFT
	$\Delta E(S_0)$	$\Delta E(S_1)$	$\Delta E(S_1)$
S_0	-0.02	4.43	4.28
S_1	0.84	3.78	3.79
$(S_0)_{DM}$	-0.02	4.39	4.25
$(S_1)_{DM}$	0.75	3.80	3.79
Excimer[b]	0.0	2.93, 4.16	2.91, 3.98

a. Acetone monomer geometries in different states used in energy calculations. Monomer energies are relative to that determined using M06-2X/cc-pVTZ.
b. Excimer excitation energies relative to the ground state energy using the excimer structure.

Table 2. Computed ground-state and excitation energies (eV) for pentacene using NOSI and TDDFT. Optimized geometries for the ground state (S_0) and the first excited state (S_1 also labeled as L_a), and the monomer geometry in the optimized excimer $(S_1)_{DM}^{mono}$ are used. The Minnesota M06-2X density functional along with the cc-pVDZ basis set is used.

Geometry[a]	NOSI			TDDFT	
	S_0	$L_a(S_1)$	$L_b(S_2)$	$L_a(S_1)$	$L_b(S_2)$
S_0	0.0	2.39	3.35	2.35	3.63
S_1	0.21	2.06	3.11	2.10	3.54
$(S_1)_{DM}^{monmer}$	0.09	2.10	3.14	2.06	3.44
Excimer[b]	0.0	0.88, 1.87	2.33, 2.49	0.87, 2.04	2.14, 2.42

a. Acetone monomer geometries in different states used in energy calculations. Monomer energies are relative to that determined using M06-2X/cc-pVDZ.
b. Excimer excitation energies relative to the ground state energy using the excimer structure.

For MS-EDA, we first consider the asymmetric acetone excimer, which was optimized for the S_1 state of the complex using TDDFT with the M06-2X functional. We obtained a structure that is best characterized as the local excitation of one monomer that is distorted at the carbonyl carbon from sp^2 hybridization (Figure 1A), forming a tail-to-tail dimer with an in-phase

combination of the distorted π^* orbital of the two acetone molecules as the highest singly occupied orbital. The vastly different monomer structures here turn out to be equivalent to a general exciplex complex if the two compounds were different. Interestingly, the distorted acetone monomer in the excimer complex, $(AA)_{S_1}$, is somewhat less deformed by about 0.1 eV (2.4 kcal/mol) than the optimized geometry, $(A)_{S_1}$, in isolation, but the adiabatic excitation energies (3.8 eV) are essentially the same (Table 1). The agreement between NOSI and TDDFT calculations is good for the four geometries considered (Table 1).

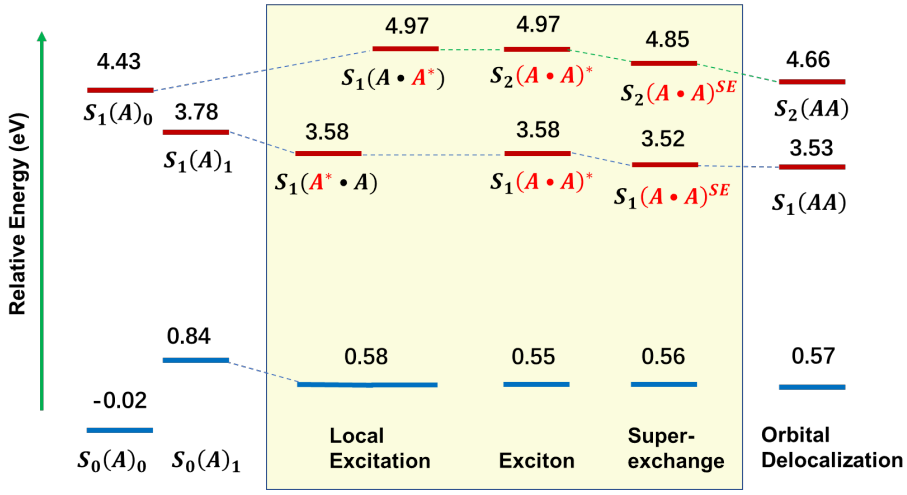

Figure 2. Computed ground and excited state energies (eV) for acetone monomer (***A***) and the excimer complex (***AA***), and the intermediate energy terms from multistate energy-decomposition analysis (MS-EDA). The energies for the fully delocalized excimer are determined using TDDFT/M06-2X. States shown in the light-yellow background are determined using nonorthogonal state interaction (NOSI) with the excimer geometry, and the excited species are indicated in red. The notations $(A)_0$ and $(A)_1$ denote the optimized structures for the ground and first excited state of acetone. Energies are given relative to that of acetone in the ground state.

Figure 2 shows the progressive change of energies for the ground state and excited states for the terms defined by eq 3. First, there is a weak binding interaction in the ground state with a ΔE_{Lint} value of -0.24 eV (-5.5 kcal/mol), giving rise to local excitation energies of 3.00 and 4.39 eV in the bimolecular complex, essentially the same as the isolated monomers in the equilibrium

S_1 and S_0 geometries at 2.95 and 4.45 eV, respectively (Table 1). Excitation energies for the monomer-in-excimer geometries are also similar (3.05 and 4.41 eV). Thus, there is a small polarization effect of less than 0.05 eV that stabilizes the excited states due to local excitation. Interestingly, state interaction among the locally excited states have little effects on the exciton states, with identical first and second excitation energies as the two locally excited states. For this excimer structure, the net exciton resonance energy is zero. Super-exchange due to mutual charge transfer does contribute to state stabilization, lowering the first and the second excited state energy by 0.06 and 0.12 eV, respectively. The magnitudes of SE stabilization in these two states are mirrored by the corresponding structural weights for the non-equivalent CT directions, amounting to 2.56% and 0.06% for the BCT (monomer 2 → monomer 1) and FCT states in the first excited state, and 0.02% and 7.54% in the second excited state. Notice the different directions of CT contributions for the two states. Finally, we found that orbital delocalization and configuration-space expansion in TDDFT calculations have little effects on the ground state (not surprisingly) and the first excited state; however, a noticeable stabilization to the second excited state of the excimer, by 0.19 eV, is obtained (Figure 2). Overall, a net binding energy of -0.23 eV (-5.3 kcal/mol) for the acetone excimer is obtained both from NOSI and TDDFT calculations.

Table 3. Computed excitation energies (eV) and energy components from multistate energy decomposition analysis (MS-EDA) for pentacene dimers in the excimer, stacked and fishbone geometries. Excitation energies are relative to that of the adiabatic ground state of isolated pentacene(s). The M06-2X density functional is used. See caption of Table 2.

Energy term	Excimer		Stacked		Fishbone[b]	
	L_a	L_b	L_a	L_b	L_a	L_b
$\Delta E_{\mathrm{Lint}}[\Psi_{(X\bullet Y)}]^a$	0.03		0.05		-0.33	
$\Delta E_{\mathrm{Lex}}[\Psi^{K_X}_{(X^*\bullet Y)}]$	1.89	3.04	2.10	3.28	2.00	2.92
$\Delta E_{\mathrm{Lex}}[\Psi^{K_Y}_{(X\bullet Y^*)}]$	1.89	3.04	2.10	3.28	1.98	2.92

$\Delta E_{\mathrm{Ex}}[\Psi^{K}_{(X\bullet Y)^{*}}]$	1.33	2.70	1.74	2.80	1.97	2.92
$\Delta E_{\mathrm{Ex}}[\Psi^{K'}_{(X\bullet Y)^{*}}]$	2.46	3.38	2.58	3.47	2.02	2.93
$\Delta E_{\mathrm{SE}}[\Psi^{K}_{(X\bullet Y)^{*}_{\pm}}]$	0.62	2.70	1.02	2.80	1.88	2.92
$\Delta E_{\mathrm{SE}}[\Psi^{K'}_{(X\bullet Y)^{*}_{\pm}}]$	2.30	3.38	2.54	3.47	1.97	2.93
$\Delta E^{K}_{\mathrm{OCD}}$	0.87	2.42	1.24	2.58	2.03	2.98
$\Delta E^{K'}_{\mathrm{OCD}}$	2.04	2.80	2.35	3.02	2.24	NA[b]

a. The ground-state binding energy for the delocalized dimers are -0.05, +0.03, and -0.47 eV for the excimer, stacked and fishbone geometries, respectively. Binding energies for the first excited-state complexes are -1.52, -1.15, and -0.36 eV in the three corresponding geometries. Much of the excited state binding energy for the fishbone configuration originate from ground-state binding.
b. The HOMO-1→LUMO+1 configuration was not included in NOSI calculations.
c. Several mixed states have close energies, not assigned to the L_b state.

We now turn to the case of pentacene excimer, which exhibits different behaviors in comparison with that in the asymmetric acetone excimer. Listed in Table 3 are the computed energy terms, including local excitation ΔE_{Lex}, exciton excitation states ΔE_{Ex}, super-exchange stabilization ΔE_{SE}, and the orbital and configuration delocalization energies ΔE_{OCD} for the excimer complex, associated with the excimer states of pentacene in three different geometrical arrangements. The first geometry corresponds to a fully optimized structure of the S_1 excimer (D_{2h} symmetry) with the shortest inter-fragment separation at 3.15 Å, the second configuration is an on-top stacked construction with the ground-state monomer geometry at 3.3 Å, and the third is derived from the pentacene crystal in a fishbone relationship used previously (Figure 1B).[67] These structures are of interest by their own rights, but the fishbone relationship is directly relevant to pentacene monolayer materials used in solar cell research.[67] However, we shall not address the mechanism of singlet fission in the present MS-EDA study; interested readers may find conclusions in an early study using MSDFT.[67]

Table 4. Computed exciton coupling (energy-splitting) $|\Delta V_{Ex}|$, and resonance energies associated with super-exchange stabilization ΔE_{SE}^{res} and orbital and configuration delocalization ΔE_{OCD}^{ad}. Energies are given in electron volts (eV).

Relative energy	Excimer		Stacked		Fishbone	
	L_a	L_b	L_a	L_b	L_a	L_b
$\|2\Delta V_{\mathrm{Ex}}\|$	1.13	0.52	0.84	0.67	0.05	0.01
$\Delta\Delta E_{\mathrm{SE}}^{res,\pm}$	-0.71	0.00	-0.72	0.00	-0.09	0.00
$\Delta\Delta E_{\mathrm{SE}}^{res,\mp}$	-0.16	0.00	-0.04	0.00	-0.05	0.00
$\Delta\Delta E_{\mathrm{OCD}}^{ad,\pm}$	+0.15	-0.28	+0.22	-0.22	+0.15	0.06
$\Delta\Delta E_{\mathrm{OCD}}^{ad,\mp}$	+0.26	-0.58	-0.19	-0.45	+0.27	NA

First, mutual polarization induced by local excitation of one monomer introduces modest effects relative to the adiabatic energies of an isolated monomer, stabilizing the L_a and L_b states of the excimer by 0.17 (2.06 vs. 1.89) and 0.07 (3.11 vs. 3.04) eV (Tables 2 and 3), respectively. This is significant in view of the non-polar nature of the hydrogen carbon system, although there is also a slight change from structural variations from the monomer to the excimer. The most striking finding from Table 3 and also in Figure 3 is the large exciton coupling energies and the resulting energy splitting both for the L_a and L_b states in the excimer and stacked structures, giving rise to exciton splitting energies $|2\Delta V_{\mathrm{Ex}}|$ of 1.13 and 0.84 eV for the L_a states, and 0.68 and 0.67 eV for the L_b states (Table 4). Interestingly, the computed exciton coupling (energy splitting) between locally excited states is fortuitously nearly identical to that determined as the energy difference between the two adiabatic states (Table 2, Figure 3). In comparison with the "solar-cell relevant" fishbone structure, the computed exciton coupling is only 0.05eV for the L_a state and 0.01 eV for the L_b state. Phase matching of the two chromophore wave functions in the dimer (excimer) complex is critical for the strength of their interaction and can have a major impact

on the energy levels.[72] This effect is clearly reflected in the tilted monomers in the fishbone complex. Thus, a small adjustment to better align the overlap of monomer wave functions may significantly enhance electronic coupling for energy and charge transfer.

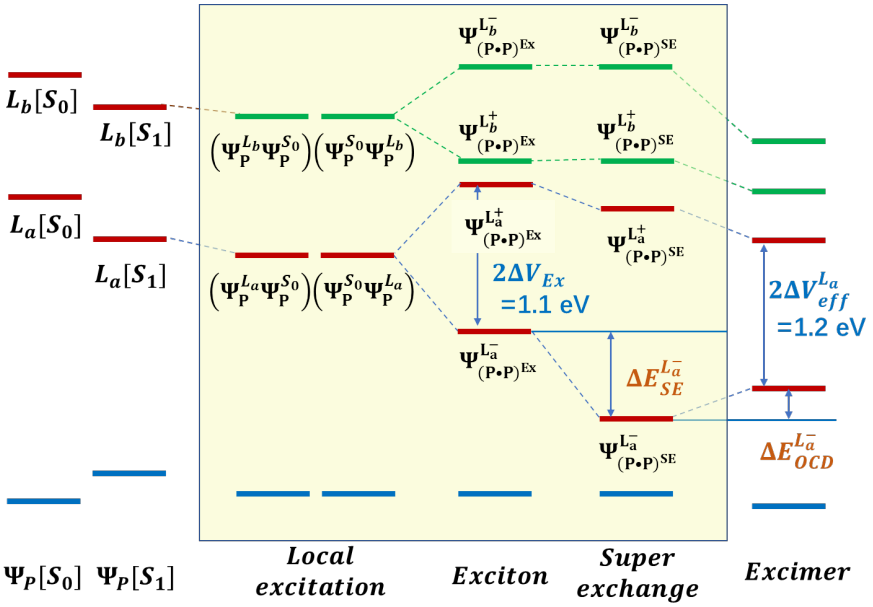

Figure 3. Computed ground and excited state energies for pentacene excimer from multistate energy-decomposition analysis (MS-EDA). States shown in light-yellow background are determined using nonorthogonal state interaction (NOSI) in MS-EDA analysis with the excimer geometry, in which excited species are indicated in red. The M06-2X density functional is used in all calculations.

A major stabilizing factor of the excimer energies comes from super-exchange. Formally, super-exchange originates from the mutual charge transfer, $|\Psi_X^+ \bullet \Psi_Y^- >$ and $|\Psi_X^- \bullet \Psi_Y^+ >$, between two monomers. However, there is no net charge transfer in the excimer complex of pentacene nor in the stacked configuration of pentacene dimer because of symmetry. Super-exchange refers to the resonance stabilization of these two CT states by mixing with the exciton states. This necessarily lowers the excimer energy relative to the corresponding exciton state because of the variational principle, which is clearly confirmed by the numerical results in Table 3. In the pentacene dimers, super-exchange stabilizes the L_a state significantly by -0.7 eV in the

excimer and stacked dimer configurations, but to a much smaller extent (-0.09 eV) in the fishbone arrangement (Table 4). Thus, phase matching of the wave functions favoring strong overlap is important to resonance mixing of inter-fragment charge transfer. In all cases, super-exchange produced no effect on the stability of the L_b state, but it does stabilize the ground state to a much smaller extent than the L_a excited states.

Finally, we comment on the effects of orbital delocalization and expansion of the configuration space in excited state calculations to yield the adiabatic ground and excited states. Unlike ground-state EDA, where orbital delocalization necessarily stabilizes the ground-state energy, the energies of the excited energies also depend on the "active space" used, which could increase or decrease the energies of a particular excited state. In principle, Hohenberg-Kohn-Sham DFT gives the exact energy of the ground state, but linear response theory introduces additional approximations. The Lu-Gao theorems of MSDFT establishes a foundation for exact excited state calculations as that of Hohenberg-Kohn theorems for the ground state.[73, 93] As in Kohn-Sham theory,[94] an approximate matrix correlation functional is needed. In a range of studies, we have found that the approximations used in the present MS-EDA analysis yield good results for excited state calculations. The computed excitation energies for the present system are within 0.2 eV of the TDDFT values (see Tables 1 and 2), and it is not clear which is more accurate without a thorough analysis. In view of the wide-spread use of the linear response theory, we have adopted the TDDFT values for the final adiabatic energies to determine the ΔE_{OCD} term in MS-EDA. For the pentacene excimer, the OCD contribution raises the energy of the first excited state, but lowers those for the higher states. Currently, we have not separated the effects from orbital and configuration expansions, which would be of interest in future studies.

An anonymous referee noted the abnormal energy increase in the ΔE_{OCD} term for the S_1 (L_a^-) state. We attribute this observation to over-stabilization by super-exchange in the present analysis, leading to an energy too low for the SE state. This issue originates from the approximate TDF energy using eq 14. MSDFT-NOSI calculations of the delocalized excimer complex show an energy splitting of 1.0 eV, in fact, slightly smaller than the value from TDDFT (1.2 eV) in Table 2 (Figure 3). In view of the $\Delta E_{\mathrm{SE}}[\Psi^K_{(X\bullet Y)^*_\pm}]$ energy term (0.62 eV) in Table 3, it is likely that the SE effect is over-estimated at least by 0.2 eV. This highlights the need to systematically develop a matrix correlation functional both for the ground and excited states.

In summary, a multistate energy decomposition analysis (MS-EDA) method is introduced to dissect the energy components in excimer complexes. Ground-state EDA, which has been extensively explored in the past, remains an active area of research. However, the development of methods for analysis of intermolecular interactions in the excited states has lagged partially because it is difficult to introduce well-defined intermediate states at higher energy levels, not to mention that the computation of excited state energies itself is challenging. Akin to an energy decomposition analysis for the ground state, the present MS-EDA provides a clear separation of energy terms that can be variationally optimized for excited-state complexes. MSDFT based on the Lu-Gao theorems provides a straightforward classification of exciton coupling, super-exchange resonance and orbital-configuration expansion. Critical to this analysis is to account for state interaction. As demonstrated in the present study, state interaction provides key insights into an understanding of excitonic coupling and super-exchange stabilization. These quantities, directly computed from the basis states of the MAS for MSDFT, rather than a *post priori* transformation, are of fundamental importance to determining the rates of electron transfer and excited state energy transfer and in applications to designing light-emitting materials. The examples highlight the roles

of state energy-matching and wave function phase-matching to the magnitude of exciton coupling and super-exchange stabilization from a perspective of well-defined diabatic states. Further, MS-EDA provides a useful tool for interpreting excited-state energies from delocalized calculations.

Supporting Information: Optimized structures used in this work (8 pages in PDF). The Supporting Information is available free of charge on the ACS Publications website at DOI:.

Acknowledgments: This work was supported in part by the Shenzhen Municipal Science and Technology Innovation Commission (KQTD2017-0330155106581) and the Key-area Research and Development Program of Guangdong Province (2020B0101350001). Computation work carried out at Minnesota has been supported by the National Institutes of Health (Grant GM046736).

References

(1) Gao, J.; Xia, X. A prior evaluation of aqueous polarization effects through Monte Carlo QM-MM simulations. *Science* **1992**, *258*, 631-635.

(2) Mo, Y.; Bao, P.; Gao, J. Energy decomposition analysis based on a block-localized wavefunction and multistate density functional theory. *Phys Chem Chem Phys* **2011**, *13*, 6760-6775.

(3) Zhao, L. L.; von Hopffgarten, M.; Andrada, D. M.; Frenking, G. Energy decomposition analysis. *WIREs Comput. Mol. Sci.* **2018**, *8*, e1345.

(4) Morokuma, K. Molecular Orbital Studies of Hydrogen Bonds .3. C=O H-O Hydrogen Bond in H2co H2o and H2co 2h2o. *J. Chem. Phys.* **1971**, *55*, 1236.

(5) Kitaura, K.; Morokuma, K. New Energy Decomposition Scheme for Molecular-Interactions within Hartree-Fock Approximation. *Int. J. Quantum Chem.* **1976**, *10*, 325-340.

(6) Morokuma, K. Why Do Molecules Interact - Origin of Electron Donor-Acceptor Complexes, Hydrogen-Bonding, and Proton Affinity. *Acc. Chem. Res.* **1977**, *10*, 294-300.

(7) Ziegler, T.; Rauk, A. Calculation of Bonding Energies by Hartree-Fock Slater Method .1. Transition-State Method. *Theor. Chim. Acta* **1977**, *46*, 1-10.

(8) Bagus, P. S.; Hermann, K.; Bauschlicher, C. W. A New Analysis of Charge-Transfer and Polarization for Ligand-Metal Bonding - Model Studies of Al4co and Al4nh3. *J. Chem. Phys.* **1984**, *80*, 4378-4386.

(9) Bagus, P. S.; Hermann, K.; Bauschlicher, C. W. On the Nature of the Bonding of Lone Pair Ligands to a Transition-Metal. *J. Chem. Phys.* **1984**, *81*, 1966-1974.

(10) Bagus, P. S.; Illas, F. Decomposition of the Chemisorption Bond by Constrained Variations - Order of the Variations and Construction of the Variational Spaces. *j. Chem. Phys.* **1992**, *96*, 8962-8970.

(11) Stevens, W. J.; Fink, W. H. Frozen fragment reduced variational space analysis of hydrogen bonding interactions. Application ot the water dimer. *Chem. Phys. Lett.* **1987**, *139*, 15-22.

(12) Glendening, E. D.; Weinhold, F. Natural resonance theory: I. General formalism. *J. Comput. Chem.* **1998**, *19*, 593-609.

(13) Gordon, M. S.; Jensen, J. H. Understanding the hydrogen bond using quantum chemistry. *Acc. Chem. Res.* **1996**, *29*, 536-543.

(14) Chen, W.; Gordon, M. S. Energy decomposition analyses for many-body interaction and applications to water complexes. *J. Phys. Chem.* **1996**, *100*, 14316-14328.
(15) Gordon, M. S.; Slipchenko, L.; Li, H.; Jensen, J. H. The effective fragment potential: a general method for predicting intermolecular interactions. *Ann. Rep. Comput. Chem.* **2007**, *3*, 177-193.
(16) Reinhardt, P.; Piquemal, J.-P.; Savin, A. Fragment-Localized Kohn-Sham Orbitals via a Singles Configuration-Interaction Procedure and Application to Local Properties and Intermolecular Energy Decomposition Analysis. *J. Chem. Theory Comput.* **2008**, *4*, 2020-2029.
(17) Wu, Q.; Ayers, P. W.; Zhang, Y. K. Density-based energy decomposition analysis for intermolecular interactions with variationally determined intermediate state energies. *J. Chem. Phys.* **2009**, *131*, 164112.
(18) Su, P. F.; Li, H. Energy decomposition analysis of covalent bonds and intermolecular interactions. *J. Chem. Phys.* **2009**, *131*, 014102.
(19) Piquemal, J. P.; Marquez, A.; Parisel, O.; Giessner-Prettre, C. A CSOV study of the difference between HF and DFT intermolecular interaction energy values: The importance of the charge transfer contribution. *J. Comput. Chem.* **2005**, *26*, 1052-1062.
(20) Gourlaouen, C.; Piquemal, J. P.; Saue, T.; Parisel, O. Revisiting the geometry of nd(10) (n+1)s(0) [M(H2O)](P+) complexes using four-component relativistic DFT calculations and scalar relativistic correlated CSOV energy decompositions (MP+=Cu+, Zn2+, Ag+, Cd2+, Au+, Hg2+). *Journal of Computational Chemistry* **2006**, *27*, 142-156.
(21) Bickelhaupt, F. M.; Baerends, E. J. In *Rev. Comput. Chem.*, lipkowitz, K. B., Boyd, D. B. Eds.; Vol. 15; Wiley-VCH, 1999; p 1.
(22) Guerra, C. F.; Bickelhaupt, F. M.; Snijders, J. G.; Baerends, E. J. The nature of the hydrogen bond in DNA base pairs: The role of charge transfer and resonance assistance. *Chem. Euro. J.* **1999**, *5*, 3581-3594.
(23) Bickelhaupt, F. M.; Baerends, E. J. The case for steric repulsion causing the staggered conformation of ethane. *Angew. Chem. Int. Ed.* **2003**, *42*, 4183-4188.
(24) Khaliullin, R. Z.; Cobar, E. A.; Lochan, R. C.; Bell, A. T.; Head-Gordon, M. Unravelling the Origin of Intermolecular Interactions Using Absolutely Localized Molecular Orbitals. *J. Phys. Chem. A* **2007**, *111*, 8753-8765.
(25) Khaliullin, R. Z.; Head-Gordon, M.; Bell, A. T. An efficient self-consistent field method for large systems of weakly interacting components. *J. Chem. Phys.* **2006**, *124*, 204105.

(26) Andres, J.; Ayers, P. W.; Boto, R. A.; Carbo-Dorca, R.; Chermette, H.; Cioslowski, J.; Contreras-Garcia, J.; Cooper, D. L.; Frenking, G.; Gatti, C.; et al. Nine questions on energy decomposition analysis. *J. Comput. Chem.* **2019**, *40*, 2248-2283.
(27) Mo, Y.; Zhang, Y.; Gao, J. A Simple Electrostatic Model for Trisilylamine: Theoretical Examinations of the n.fwdarw..sigma. Negative Hyperconjugation, p.pi..fwdarw.d.pi. Bonding, and Stereoelectronic Interaction. *J. Am. Chem. Soc.* **1999**, *121*, 5737-5742.
(28) Mo, Y.; Gao, J.; Peyerimhoff, S. D. Energy decomposition analysis of intermolecular interactions using a block-localized wave function approach. *J. Chem. Phys.* **2000**, *112*, 5530-5538.
(29) Mo, Y.; Schleyer, P. v. R.; Wu, W.; Lin, M.; Zhang, Q.; Gao, J. Importance of Electronic Delocalization on the C-N Bond Rotation in HCX(NH2) (X = O, NH, CH2, S, and Se). *J. Phys. Chem. A* **2003**, *107*, 10011-10018.
(30) Mo, Y.; Gao, J. Polarization and Charge-Transfer Effects in Aqueous Solution via Ab Initio QM/MM Simulations. *J. Phys. Chem. B* **2006**, *110*, 2976-2980.
(31) Mo, Y. R. Computational evidence that hyperconjugative interactions are not responsible for the anomeric effect. *Nat Chem* **2010**, *2*, 666-671.
(32) Frenking, G.; Loschen, C.; Krapp, A.; Fau, S.; Strauss, S. H. Electronic structure of CO - An exercise in modern chemical bonding theory. *J. Comput. Chem.* **2007**, *28*, 117-126.
(33) Frenking, G.; Frohlich, N. The nature of the bonding in transition-metal compounds. *Chem. Rev.* **2000**, *100*, 717-774.
(34) Michalak, A.; Mitoraj, M.; Ziegler, T. Bond orbitals from chemical valence theory. *J. Phys. Chem. A* **2008**, *112*, 1933-1939.
(35) Kurczab, R.; Mitoraj, M. P.; Michalak, A.; Ziegler, T. Theoretical Analysis of the Resonance Assisted Hydrogen Bond Based on the Combined Extended Transition State Method and Natural Orbitals for Chemical Valence Scheme. *J. Phys. Chem. A* **2010**, *114*, 8581-8590.
(36) Dederichs, P. H.; Bluegel, S.; Zeller, R.; Akai, H. Ground states of constrained systems: application to cerium impurities. *Phys. Rev. Lett.* **1984**, *53*, 2512-2515.
(37) Francisco, E.; Pendas, A. M.; Blanco, M. A. A molecular energy decomposition scheme for atoms in molecules. *J. Chem. Theory Comput.* **2006**, *2*, 90-102.
(38) Liu, S. N.; Govind, N.; Pedersen, L. G. Exploring the origin of the internal rotational barrier for molecules with one rotatable dihedral angle. *J. Chem. Phys.* **2008**, *129*, 094104.
(39) Stone, A. J. *The Theory of Intermolecular Forces*; Oxford University Press, 1996.

(40) Jeziorski, B.; Moszynski, R.; Szalewicz, K. Perturbation Theory Approach to Intermolecular Potential Energy Surfaces of van der Waals Complexes. *Chem. Rev.* **1994**, *94*, 1887-1930.
(41) Misquitta, A. J.; Szalewicz, K. Symmetry-adapted perturbation-theory calculations of intermolecular forces employing density-functional description of monomers. *J. Chem. Phys.* **2005**, *122*, 214109.
(42) Shahbaz, M.; Szalewicz, K. Dispersion Energy from Local Polarizability Density. *Phys. Rev. Lett.* **2019**, *122*, 213001.
(43) Xantheas, S. S. On the importance of the fragment relaxation energy terms in the estimation of the basis set superposition error correction to the intermolecular interaction energy. *J. Chem. Phys.* **1996**, *104*, 8821-8824.
(44) Angeli, C.; Cimiraglia, R.; Malrieu, J. P. On the relative merits of non-orthogonal and orthogonal valence bond methods illustrated on the hydrogen molecule. *J Chem Educ* **2008**, *85*, 150-158.
(45) Schneider, W. B.; Bistoni, G.; Sparta, M.; Saitow, M.; Riplinger, C.; Auer, A. A.; Neese, F. Decomposition of Intermolecular Interaction Energies within the Local Pair Natural Orbital Coupled Cluster Framework. *J. Chem. Theory Comput.* **2016**, *12*, 4778-4792.
(46) Altun, A.; Saitow, M.; Neese, F.; Bistoni, G. Local Energy Decomposition of Open-Shell Molecular Systems in the Domain-Based Local Pair Natural Orbital Coupled Cluster Framework. *J. Chem. Theory Comput.* **2019**, *15*, 1616-1632.
(47) Horn, P. R.; Mao, Y. Z.; Head-Gordon, M. Probing non-covalent interactions with a second generation energy decomposition analysis using absolutely localized molecular orbitals. *Phys Chem Chem Phys* **2016**, *18*, 23067-23079.
(48) Levine, D. S.; Horn, P. R.; Mao, Y. Z.; Head-Gordon, M. Variational Energy Decomposition Analysis of Chemical Bonding. 1. Spin-Pure Analysis of Single Bonds. *J. Chem. Theory Comput.* **2016**, *12*, 4812-4820.
(49) Mao, Y. Z.; Loipersberger, M.; Horn, P. R.; Das, A.; Demerdash, O.; Levine, D. S.; Veccham, S. P.; Head-Gordon, T.; Head-Gordon, M. From Intermolecular Interaction Energies and Observable Shifts to Component Contributions and Back Again: A Tale of Variational Energy Decomposition Analysis. *Ann. Rev. Phys. Chem.* **2021**, *72*, 641-666.

(50) Veccham, S. P.; Lee, J.; Mao, Y. Z.; Horn, P. R.; Head-Gordon, M. A non-perturbative pairwise-additive analysis of charge transfer contributions to intermolecular interaction energies. *Phys Chem Chem Phys* **2021**, *23*, 928-943.
(51) Shen, H. Y.; Wang, Z. L.; Head-Gordon, M. Generalization of ETS-NOCV and ALMO-COVP Energy Decomposition Analysis to Connect Any Two Electronic States and Comparative Assessment. *J. Chem. Theory Comput.* **2022**, *18*, 7428–7441.
(52) Han, J. T.; Grofe, A.; Gao, J. L. Variational Energy Decomposition Analysis of Charge-Transfer Interactions between Metals and Ligands in Carbonyl Complexes. *Inorg. Chem.* **2021**, *60*, 14060-14071.
(53) Mathew, P. T.; Fang, F. Z. Periodic energy decomposition analysis for electronic transport studies as a tool for atomic scale device manufacturing. *Int. J. Extr. Manufact.* **2020**, *2*, 015401.
(54) Xu, Y.; Zhang, S.; Lindahl, E.; Friedman, R.; Wu, W.; Su, P. F. A general tight-binding based energy decomposition analysis scheme for intermolecular interactions in large molecules. *J. Chem. Phys.* **2022**, *157*, 034104.
(55) Chen, H.; Skylaris, C. K. Energy decomposition analysis method for metallic systems. *Phys Chem Chem Phys* **2022**, *24*, 1702-1711.
(56) Ge, Q. H.; Mao, Y. Z.; Head-Gordon, M. Energy decomposition analysis for exciplexes using absolutely localized molecular orbitals. *J. Chem. Phys.* **2018**, *148*, 064105.
(57) Closser, K. D.; Ge, Q. H.; Mao, Y. Z.; Shao, Y. H.; Head-Gordon, M. Superposition of Fragment Excitations for Excited States of Large Clusters with Application to Helium Clusters. *J. Chem. Theory Comput.* **2015**, *11*, 5791-5803.
(58) Stoll, H.; Wagenblast, G.; Preuss, H. On the use of local basis sets for localized molecular orbitals. *Theor. Chim. Acta* **1980**, *57*, 169-178.
(59) Ge, Q. H.; Head-Gordon, M. Energy Decomposition Analysis for Excimers Using Absolutely Localized Molecular Orbitals within Time-Dependent Density Functional Theory and Configuration Interaction with Single Excitations. *J. Chem. Theory Comput.* **2018**, *14*, 5156-5168.
(60) Song, L.; Gao, J. On the Construction of Diabatic and Adiabatic Potential Energy Surfaces Based on Ab Initio Valence Bond Theory. *J. Phys. Chem. A* **2008**, *112*, 12925-12935.
(61) Grofe, A.; Qu, Z. X.; Truhlar, D. G.; Li, H.; Gao, J. Diabatic-At-Construction Method for Diabatic and Adiabatic Ground and Excited States Based on Multistate Density Functional Theory. *J. Chem. Theory Comput.* **2017**, *13*, 1176-1187.

(62) Liu, M.; Chen, X.; Grofe, A.; Gao, J. Diabatic States at Construction (DAC) through Generalized Singular Value Decomposition. *J Phys Chem Lett* **2018**, *9*, 6038-6046.
(63) Li, H.; Wang, Y. J.; Ye, M. P.; Li, S. S.; Li, D. Y.; Ren, H. S.; Wang, M.; Du, L. C.; Li, H.; Veglia, G.; et al. Dynamical and allosteric regulation of photoprotection in light harvesting complex II. *Sci China Chem* **2020**, *63*, 1121-1133.
(64) Li, X.; Ren, H.; Kundu, M.; Liu, Z.; Zhong, F. W.; Wang, L.; Gao, J.; Zhong, D. A leap in quantum efficiency through light harvesting in photoreceptor UVR8. *Nat. Commun.* **2020**, *11*, 1-9.
(65) Li, X. K.; Liu, Z. Y.; Ren, H. S.; Kundu, M.; Wang, L. J.; Gao, J. L.; Zhong, D. P. Dynamics and mechanism of light harvesting in UV photoreceptor UVR8. *Chem. Sci.* **2020**, *11*, 12553-12569.
(66) Li, X. K.; Liu, Z. Y.; Ren, H. S.; Kundu, M.; Zhong, F. W.; Wang, L. J.; Gao, J. L.; Zhong, D. P. Dynamics and mechanism of dimer dissociation of photoreceptor UVR8. *Nature Comm.* **2022**, *13*, 10.1038/s41467-41021-27756-w.
(67) Chan, W.-L.; Berkelbach, T. C.; Provorse, M. R.; Monahan, N. R.; Tritsch, J. R.; Hybertsen, M. S.; Reichman, D. R.; Gao, J.; Zhu, X.-Y. The quantum coherent mechanism for singlet fission: Experiment and theory. *Acc. Chem. Res.* **2013**, *46*, 1321–1329.
(68) Yue, L.; Liu, Y. J. Conical Intersection in Chemiluminescence of Cyclic Peroxides. *J. Phys. Chem. Lett.* **2022**, *13*, 10671-10687.
(69) Cembran, A.; Song, L.; Mo, Y.; Gao, J. Block-localized density functional theory (BLDFT), diabatic coupling, and its use in valence bond theory for representing reactive potential energy surfaces. *J. Chem. Theory Comput.* **2009**, *5*, 2702-2716.
(70) Frenkel, J. On the transformation of light into heat in solids. I. *Phys. Rev.* **1931**, *37*, 17-44.
(71) Zhao, R.; Grofe, A.; Wang, Z.; Bao, P.; Chen, X.; Liu, W.; Gao, J. Dynamic-then-Static Approach for Core Excitations of Open-Shell Molecules. *J. Phys. Chem. Lett.* **2021**, *12*, 7409-7417.
(72) Zhao, R. Q.; Hettich, C. P.; Chen, X.; Gao, J. L. Minimal-active-space multistate density functional theory for excitation energy involving local and charge transfer states. *NPJ Comput. Mater.* **2021**, *7*, 148.
(73) Lu, Y. Y.; Gao, J. L. Multistate Density Functional Theory of Excited States. *J. Phys. Chem. Lett.* **2022**, *13*, 7762-7769.

(74) Lu, Y. Y.; Gao, J. L. Fundamental Variable and Density Representation in Multistate DFT for Excited States. *J. Chem. Theory Comput.* **2022**, *18*, 7403-7411.
(75) Mo, Y.; Gao, J. Ab initio QM/MM simulations with a molecular orbital-valence bond (MOVB) method: application to an SN2 reaction in water. *J. Comput. Chem.* **2000**, *21*, 1458-1469.
(76) Mo, Y.; Gao, J. An Ab Initio Molecular Orbital-Valence Bond (MOVB) Method for Simulating Chemical Reactions in Solution. *J. Phys. Chem. A* **2000**, *104*, 3012-3020.
(77) Lu, Y. Y.; Zhao, R. Q.; Zhang, J.; Liu, M. Y.; Gao, J. L. Minimal Active Space: NOSCF and NOSI in Multistate Density Functional Theory. *J. Chem. Theory Comput.* **2022**, *18*, 6407-6420.
(78) Bao, P.; Hettich, C. P.; Shi, Q.; Gao, J. Block-Localized Excitation for Excimer Complex and Diabatic Coupling. *J. Chem. Theory Comput.* **2021**, *17*, 240-254.
(79) Grofe, A.; Zhao, R.; Wildman, A.; Stetina, T. F.; Li, X.; Bao, P.; Gao, J. Generalization of Block-Localized Wave Function for Constrained Optimization of Excited Determinants. *J. Chem. Theory Comput.* **2021**, *17*, 277-289.
(80) Zhao, Y.; Truhlar, D. G. M06 DFT functionals. *Theor. Chem. Acc.* **2008**, *120*, 215.
(81) Chirgwin, H. B.; Coulson, C. A. The electronic structure of conjugated systems. VI. *Proc. R. Soc. London Ser. A* **1950**, *201*, 196-209.
(82) Zarea, M.; Powell, D.; Renaud, N.; Wasielewski, M. R.; Ratner, M. A. Decoherence and Quantum Interference in a Four-Site Model System: Mechanisms and Turnovers. *J. Phys. Chem. B* **2013**, *117*, 1010-1020.
(83) Gao, J.; Grofe, A.; Ren, H.; Bao, P. Beyond Kohn–Sham Approximation: Hybrid Multistate Wave Function and Density Functional Theory. *J. Phys. Chem. Lett.* **2016**, *7*, 5143-5149.
(84) Grofe, A.; Chen, X.; Liu, W.; Gao, J. Spin-Multiplet Components and Energy Splittings by Multistate Density Functional Theory. *J. Phys. Chem. Lett.* **2017**, *8*, 4838-4845.
(85) Yang, L. K.; Grofe, A.; Reimers, J.; Gao, J. Multistate density functional theory applied with 3 unpaired electrons in 3 orbitals: The singdoublet and tripdoublet states of the ethylene cation. *Chem. Phys. Lett.* **2019**, *736*, 136803.
(86) King, H. F.; Staton, R. E.; Kim, H.; Wyatt, R. E.; Parr, R. G. Corresponding orbitals and the nonorthogonality problems in molecular quantum mechanics. *J. Chem. Phys.* **1967**, *47*, 1936-1941.
(87) Zhang, J.; Pan, Z.; Zhao, R.; Hou, X.; Zhang, X.; Tang, Z.; Zhang, Y.; Wu, Y.; Liu, W.; Gao, J. *Qbics - Quantum biology, informatics and chemistry server.*; Shenzhen Bay Laboratory: Shenzhen, China, 2023.

(88) Schmidt, M. W.; Baldridge, K. K.; Boatz, J. A.; Elbert, S. T.; Gordon, M. S.; Jensen, J. H.; Koseki, S.; Matsunaga, N.; Nguyen, K. A.; Su, S. J.; et al. *GAMESS*; 1993.

(89) Dunning, T. H., Jr. Gaussian basis sets for use in correlated molecular calculations. I. The atoms boron through neon and hydrogen. *J. Chem. Phys.* **1989**, *90*, 1007-1023.

(90) Frisch, M. J.; Trucks, G. W.; Schlegel, H. B.; Scuseria, G. E.; M. A. Robb; etc. *Gaussian 16*; Gaussian, Inc.: Wallingford CT, 2016., 2016.

(91) Aidas, K.; Mikkelsen, K. V.; Mennucci, B.; Kongsted, J. Fluorescence and Phosphorescence of Acetone in Neat Liquid and Aqueous Solution Studied by QM/MM and PCM Approaches. *Int. J. Quantum Chem.* **2011**, *111*, 1511-1520.

(92) Osullivan, M.; Testa, A. C. Monomer and Excimer Emission of Acetone. *J. Am. Chem. Soc.* **1968**, *90*, 6245-6246.

(93) Hohenberg, P.; Kohn, W. Inhomogeneous electron gas. *Phys. Rev.* **1964**, *136*, B864.

(94) Kohn, W.; Sham, L. J. Self-consistent equations including exchange and correlation effects. *Phys. Rev.* **1965**, *140*, A1133.